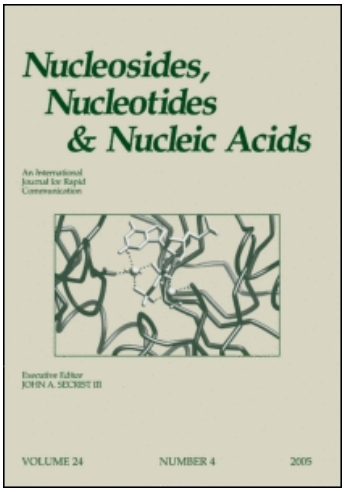

Nucleosides, Nucleotides and Nucleic Acids
Publication details, including instructions for authors and subscription information:
http://www.informaworld.com/smpp/title~content=t713597286

X-Ray Crystallographic and Kinetic Analysis of Human Purine Nucleoside Phosphorylase Complexes with 1-β-D-Ribofuranosyl-1,2,4-triazole-3-carobxamide and 1-β-D-Ribofuranosyl-1,2,4-triazole-3-carboxamidine

Richard L. Walter[a]; Jindrich Symersky[a]; Anne F. Poirot[b]; Johanna D. Stoeckler[b]; Mark D. Erionf[c]; Steven E. Ealick[a]
[a] Section of Biochemistry, Molecular and Cell Biology, Cornell University, Ithaca, New York [b] Section of Molecular and Biochemical Pharmacology, Brown University, Providence, Rhode Island [c] Central Research Laboratories, CIBA-Geigy, Ltd., Basel, Switzerland

To cite this Article Walter, Richard L. , Symersky, Jindrich , Poirot, Anne F. , Stoeckler, Johanna D. , Erionf, Mark D. and Ealick, Steven E.(1994) 'X-Ray Crystallographic and Kinetic Analysis of Human Purine Nucleoside Phosphorylase Complexes with 1-β-D-Ribofuranosyl-1,2,4-triazole-3-carobxamide and 1-β-D-Ribofuranosyl-1,2,4-triazole-3-carboxamidine', Nucleosides, Nucleotides and Nucleic Acids, 13: 1, 689 — 706
To link to this Article: DOI: 10.1080/15257779408013273
URL: http://dx.doi.org/10.1080/15257779408013273

NUCLEOSIDES & NUCLEOTIDES, 13(1-3), 689-706 (1994)

X-RAY CRYSTALLOGRAPHIC AND KINETIC ANALYSIS OF HUMAN PURINE NUCLEOSIDE PHOSPHORYLASE COMPLEXES WITH 1-β-D-RIBOFURANOSYL-1,2,4-TRIAZOLE-3-CARBOXAMIDE AND 1-β-D-RIBOFURANOSYL-1,2,4-TRIAZOLE-3-CARBOXAMIDINE

Richard L. Walter‡, Jindrich Symersky‡, Anne F. Poirot§, Johanna D. Stoeckler§, Mark D. Erion¶ and Steven E. Ealick‡*

‡Section of Biochemistry, Molecular and Cell Biology, Cornell University, Ithaca, New York 14853, §Section of Molecular and Biochemical Pharmacology, Brown University, Providence, Rhode Island 02912 and ¶Central Research Laboratories, CIBA-Geigy, Ltd., Basel, Switzerland, * To whom correspondence should be addressed.

ABSTRACT

The three-dimensional structures of the complexes between human erythrocytic purine nucleoside phosphorylase (PNP) and both 1-β-D-ribofuranosyl-1,2,4-triazole-3-carboxamide (ribavirin) and 1-β-D-ribofuranosyl-1,2,4-triazole-3-carboxamidine (TCNR) have been determined using X-ray crystallographic techniques. The structures have been refined at 2.9 Å resolution using simulated annealing and conjugate-gradient minimization techniques to an R value of 21.8% for ribavirin and 20.8% for TCNR. Ribavirin and TCNR are truncated nucleosides corresponding to adenosine and inosine, respectively, and are of potential interest as PNP inhibitors. Kinetic parameters have been determined for recombinant wild-type PNP and for a mutant PNP in which Asn 243 is converted to Asp. The K_i value for ribavirin is 4.9 mM with wild-type PNP and 4.7 mM with the Asn243Asp mutant, while the K_i values for TCNR are 17.6 μM and 3.8 μM with wild-type and mutant, respectively. X-ray crystallographic studies showed that the binding geometry for both of these substrate analogues was similar to that seen for natural substrates. The glycosidic torsion angles (χ) were -34° for ribavirin and -39° for TCNR which are in good agreement with values seen for other studied nucleoside complexes with PNP, but which are unusual when compared to those seen for free nucleic acid derivatives. Based upon the three-dimensional structure, interactions of Asn 243 and Glu 201 with a protonated carboxamidine of TCNR explain the stronger inhibition of PNP observed for TCNR over ribavirin.

INTRODUCTION

Purine nucleoside phosphorylase (E.C. 2.4.2.1; PNP) catalyzes the reversible phosphorolysis of purine nucleosides and 2'-deoxyribonucleosides to the free bases and (2-deoxy)ribose 1-phosphate (1). The human enzyme is specific for 6-oxopurines such as

Dedicated to the memory of Dr. Roland K. Robins

hypoxanthine and guanine and reacts only very slowly with adenine or other 6-aminopurines. Although the equilibrium constant favors nucleoside synthesis, the reverse reaction predominates in intact cells because of the relative concentrations of reactants and products:

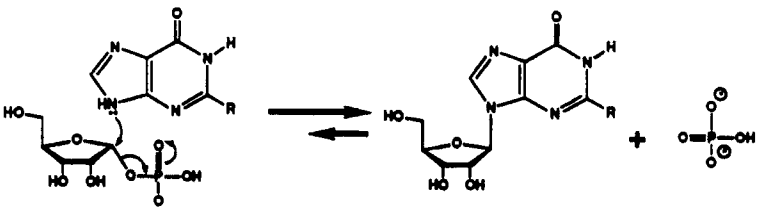

In vivo, PNP functions in the salvage pathway as an alternative to *de novo* synthesis of purine nucleotides. Due to this key role in purine nucleotide metabolism, PNP has long been a potential chemotherapeutic target. Because of the presence of PNP at high levels of activity in red blood cells and because so many purine nucleoside analogs are PNP substrates, many potential chemotherapeutic agents are cleaved by PNP and thereby inactivated. These include compounds with anti-cancer activity such as arabinosylguanine, 2'-deoxy-6-thioguanosine, 2'-deoxy-6-mercaptopurine riboside, and the anti-HIV drug 2',3'-dideoxyinosine (2).

Additional interest in PNP was stimulated by reports of a genetically related PNP deficiency in which the affected patients have little or no PNP activity. Consequently, the inability to degrade 2'-deoxyguanosine results in the accumulation of cytotoxic levels of the triphosphate (dGTP) in certain lymphocytes (3). The absence of PNP activity has been associated with a severe T-cell immune deficiency in which B-cell activity remains normal or in some cases slightly elevated. This profile suggests that PNP inhibitors might be useful in the treatment of T-cell leukemias or lymphomas, to counter T-cell mediated autoimmune diseases such as rheumatoid arthritis or systemic lupus erythematosus and to prevent organ rejection after transplantation (3).

Structurally, human PNP is a homotrimer with 289 amino acids per subunit and a total molecular weight of about 97,000 daltons. The X-ray crystal structures of human erythrocytic PNP and its guanine complex have been determined (4). The structure of human PNP (Figure 1) showed that each of the three subunits is composed of two β sheets, which pack together to form a distorted β barrel, and seven α helices. Each of the three identical active sites is located near the β barrel at the interface between adjacent subunits. The active site consists of residues from seven different segments of the amino acid sequence of one subunit and Phe 159 of the adjacent subunit. About 15 amino acid side chains make contact with the substrates and are directly involved in binding and catalysis (4).

The purine binding site is made up from residues Glu 201 and Asn 243 which provide hydrogen bonds and Ala 116, Ala 117, Phe 200, Val 217, Met 219, and Val 245. The ribose binding site is composed from residues Tyr 88 and His 257 which contribute hydrogen bonds and Phe 159 and Met 219 which provide further contacts. The phosphate binding site maps to one of the most electropositive regions in the protein and is composed primarily of the residues Ser 33, Arg 84, His 86, and Ser 220.

Because of the potential value of PNP as a chemotherapeutic target, a significant effort has been directed towards synthesizing PNP inhibitors (1,2). Among the most potent PNP inhibitors currently available are 9-substituted 9-deazapurines and multisubstrate analogs (5). These clinically promising PNP inhibitors were preceded by a group of first generation PNP inhibitors that included 8-aminoguanine, 5'-iodoformycin B, 5'-iodo-9-deazainosine and TCNR. Both TCNR (6,7) and the potent antiviral agent ribavirin (8,9,10,11) are truncated nucleosides related to 5-amino-1-β-D-ribofuranosylimidazole-4-carboxamide 5'-phosphate, an intermediate in *de novo* purine synthesis:

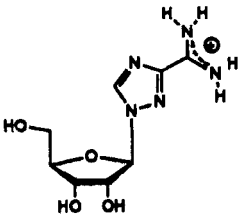

TCNR

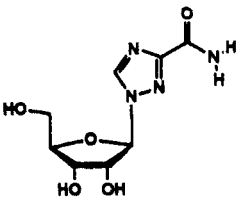

RIBAVIRIN

Interestingly, ribavirin, which is a substrate analog, is a poor inhibitor of PNP while TCNR binds to PNP more tightly than either the natural nucleoside substrates or adenosine, which shows less than 0.01% of the reactivity observed for inosine or guanosine (7,12,13). The purpose of this study is to describe structure activity relationships for TCNR and the related analog ribavirin. Complexes of these two compounds with human erythrocytic PNP were analyzed by X-ray crystallographic techniques. Also, the inhibitory activities of TCNR and ribavirin were determined both with human recombinant wild-type PNP and the related mutant, Asn243Asp, which, in general, exhibits a two-fold preference for 6-aminopurine substrates.

MATERIALS AND METHODS

Crystallization

Human erythrocytic PNP was obtained as a 25% pure lyophilized powder from a commercial source (Sigma Chemical Co., St. Louis, MO). The protein was further chromatographically purified to a level suitable for crystallization as previously described

(2,4). Purified PNP so obtained was diluted to a final concentration of 14.7 mg/ml in PO_4-buffer (pH 7.0) and crystallized by hanging drop vapor diffusion essentially as previously described (4,14). Briefly, 1.0 ml wells containing 30-32% saturated ammonium sulfate and 0.004 M dithiothreitol (Sigma Chemical Co., St. Louis, MO) in 0.05 M citrate buffer, pH 5.2-5.4, were equilibrated against 4 μl protein-containing drops by vapor diffusion in 24-well Linbro plates. The drops consisted of 2 μl of the protein solution mixed with 2 μl of the well solution on siliconized coverslips. The coverslips were then inverted over the wells and sealed by vacuum grease. Equilibration was allowed to occur for 1-2 weeks at room temperature (24°C) after which time rhombohedral-shaped crystals with dimensions up to 0.6 mm were obtained (1 to 3 crystals per drop). Crystal properties were subsequently found to be those previously reported (4): space group R32, hexagonal parameters, a = b = 142.9 Å, c = 165.3 Å, $\alpha = \beta = 90°$, $\gamma = 120°$. Crystals were prepared for data collection by transfer to a stabilizing mother liquor consisting of 60% saturated ammonium sulfate in 0.05 M citrate buffer at growth pH. Soaks of TCNR (gift of Roland K. Robins) and ribavirin (Viratek, Costa Mesa, CA) were set up at 4 mM in stabilizing mother liquor and single crystals were soaked for 24 hours immediately prior to data collection. For data collection, crystals were mounted in siliconized glass capillaries.

X-ray Crystallography

Data were collected from a single crystal for TCNR and from two crystals for ribavirin on a Xuong-Hamlin style twin detector system (San Diego Multiwire Systems, San Diego, CA). Monochromatic CuK_α X-rays (1.54184 Å) were provided by a Rigaku RU-200B rotating anode generator (Rigaku U.S.A., Danvers, MA) operating at 100 mA and 40 kV. The X-ray beam was reflected from a graphite crystal to produce monochromatic radiation and collimated by a 0.5 mm aperture pinhole collimator. All three data crystals were approximately 0.45 mm in their largest dimensions and were oriented with their largest faces against the glass capillaries. The detectors were symmetrically offset by 18° relative to the direct beam and the crystal to detector distances were 780 mm and 720 mm, respectively. This geometry gave 3.0 Å data at the farthest edges and 2.90 Å data at the detector corners. Data were collected at room temperature (24° C) using ω-scans consisting of 0.1° steps for 40 sec for TCNR and 60 sec for ribavirin. A total of 160° of data were collected for each data set. The intensity data were indexed, integrated, scaled, and merged using San Diego Multiwire Systems software. Final statistics for both data sets are as recorded in Table 1.

Model Building and Refinement:

Relative Wilson plots were used to scale complex data to a native PNP data set previously collected. After scaling, fractional changes in overall intensity from native of

Table I. X-ray Data Statistics for PNP Complexed with TCNR and Ribavirin

DATA SET	RESOLUTION SHELLS (Å)					
	OVERALL	20-5.1	5.1-4.0	4.0-3.5	3.5-3.2	3.2-2.9
TCNR						
Reflections Measured	59,403	16,979	14,413	12,136	10,771	5104
Unique Reflections	10,614	2224	2205	2237	2239	1709
Completeness (%)	76	77	79	81	81	63
Average I/σ	12.7	29.8	18.7	7.2	3.7	1.9
R_{sym} (%)*	9.5	4.3	7.1	14.7	24.9	35.4
Ribavirin						
Reflections Measured	58,951	16,939	14,309	11,981	10,654	5068
Unique Reflections	11,724	2446	2515	2473	2439	1851
Completeness (%)	85	86	91	91	90	68
Average I/σ	10.4	25.0	14.4	5.8	3.2	1.7
R_{sym} (%)*	10.6	5.7	8.3	17.2	26.7	33.2

*$R_{sym} = \Sigma | \langle I \rangle - I | / \Sigma \langle I \rangle$ summed for all observations of all reflections.

13.1% and 12.9% were observed for TCNR and ribavirin data, respectively, which are typical values for PNP inhibitor complexes. Difference Fourier maps were calculated using all data between 15-3.0 Å resolution for both complexes and between the two complexes using $|F_{O(complex)}-F_{O(native)}|$ or $|F_{O(complex1)}-F_{O(complex2)}|$ as coefficients. Calculated phases were used for data between 5 Å and 3 Å resolution and MIR phases were used for data between 15-5 Å resolution. Map peaks up to 12.6 and 12.4 times the root mean square background of the map were seen for TCNR and ribavirin, respectively, and the coordinates of these peaks matched those previously published for the PNP nucleoside binding site (4).

Electron density maps were displayed on a Silicon Graphics V6X 4D/440 workstation using the interactive graphics program CHAIN (15). The previously refined model of native PNP was used as a source of initial protein atom coordinates while initial coordinates for TCNR (6) and ribavirin (16) were obtained from the Cambridge small molecule data base (coordinates for TCNR were obtained by deleting the amino group from 5-amino-1-β-D-ribofuranosyl-1,2,4-triazole-3-carboxamidine, 5-aminoTCNR). The nucleosides and binding-induced changes to the protein structure were hand fit using peaks in the difference maps as guides. After the best visual fit was obtained the models were prepared for refinement with the XPLOR package (17). Refinement progressed as noted in Table II. Briefly, each model was first refined by a round of simulated annealing using 8-2.9 Å data with $|F| > 2\sigma(F)$ (number of reflections as shown in Table II). Simulated annealing was done essentially as described in the XPLOR tutorial files with these exceptions: an initial temperature of 4000 K and a timestep of 0.25 fsec were used. Essentially unmodified versions of the XPLOR provided tophcsdx.pro and parhcsdx.pro topology and parameter files were used for protein refinement parameters. Topology and parameter files were generated for the nucleosides using the provided toph11.dna and param11.dna modified to reflect the X-ray experimentally derived constants for TCNR and ribavirin (6,16). After simulated annealing, $2F_O-F_C$ maps (calculated phases) using 8-2.9 Å data ($|F| > 2\sigma(F)$) were calculated using the refined model, and these maps, as well as the original difference maps, were used to guide refitting of both the protein and ligand models. After refitting, the model was refined using restrained conjugate gradient minimization. For this refinement, 6-2.9 Å data with $|F| > 2\sigma(F)$ were used. Again, $2F_O-F_C$ maps were calculated and used to guide model changes, which were minimal at this point. A final cycle of conjugate gradient minimization was carried out as described above and no further drop was seen in R-factor and no additional changes were suggested from the resulting $2F_O-F_C$ maps. Root mean square deviation from ideality for geometry of these final models was calculated using XPLOR (Table II).

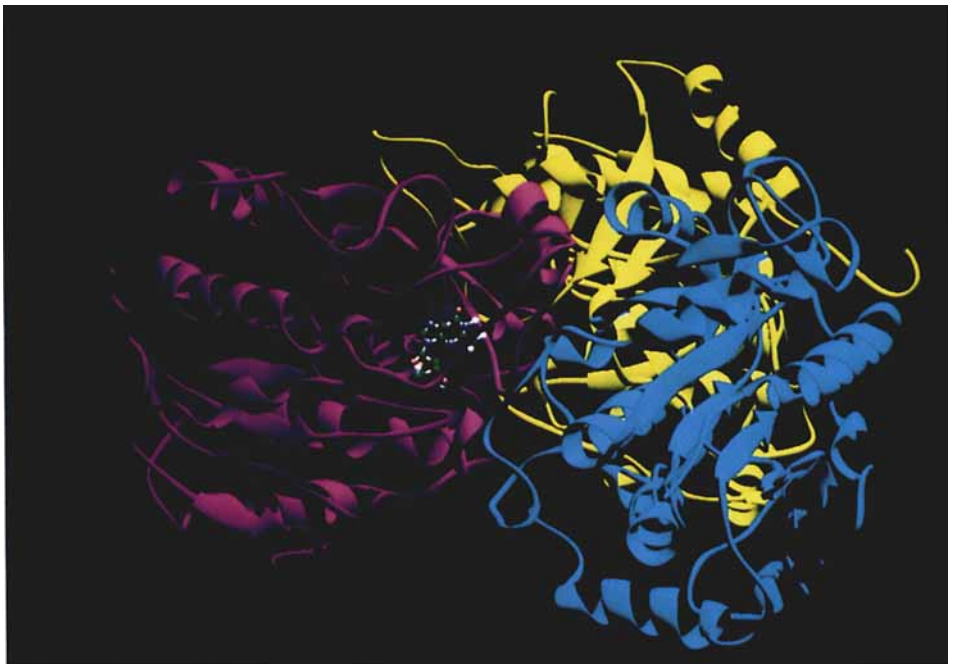

Figure 1. Ribbon diagram showing the trimeric structure of human erythrocytic purine nucleoside phosphorylase (PNP). Individual monomers are colored violet, aqua, and gold. The crystallographic threefold axis is approximately vertical. One of the three catalytically competent monomers is shown with its active site occupied by a normal substrate, guanosine.

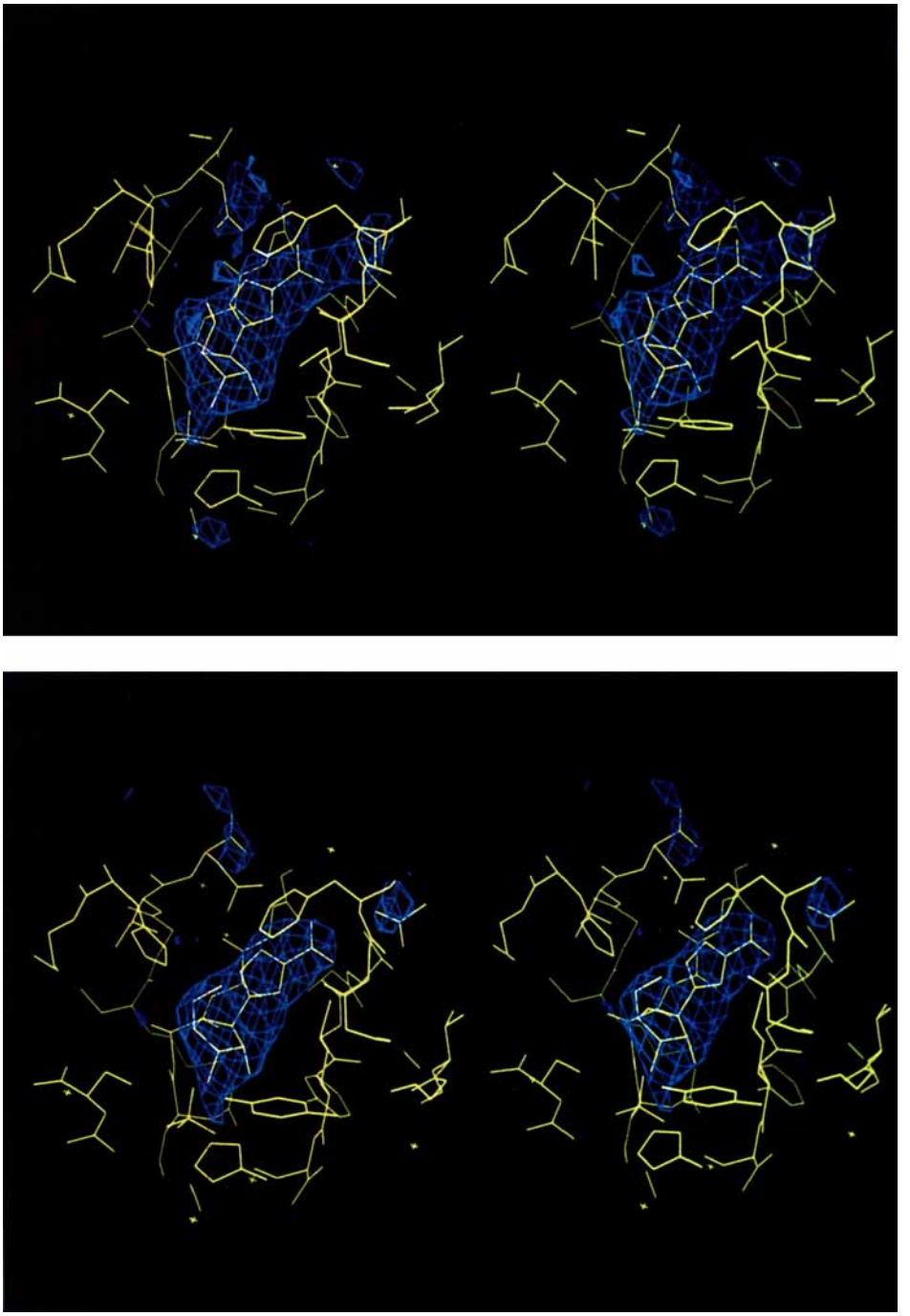

Figure 2. Side-by-side stereo figures of experimental electron density maps with final refined models showing the active site region of PNP complexed with ribavirin (upper) and TCNR (lower). Maps were calculated using $F_{o(complex)}$-$F_{o(native)}$ as coefficients and combined native phases using 15–3.0 Å data with a $F>2\sigma(F)$. Phe 159 has been removed from both figures for clarity. Both maps show virtually identical binding orientations for the two compounds and significant peaks for Glu 201 and Asn 243 interactions.

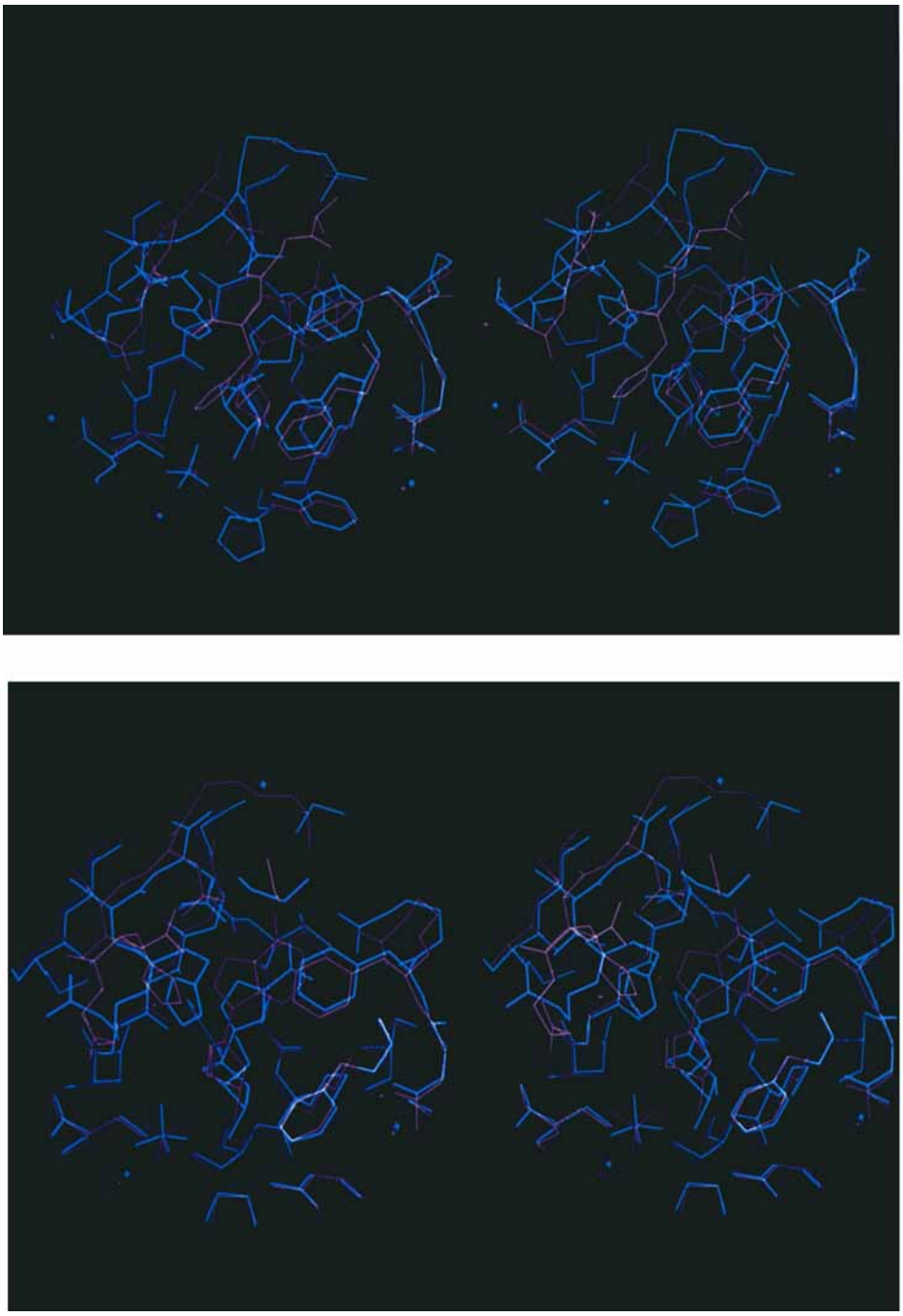

Figure 4. Side-by-side stereo diagrams of the PNP active site showing comparisons of the X-ray crystallographically determined structures of TCNR (cyan) and adenosine (violet) (lower) and ribavirin (cyan) and 9-deazainosine (violet), a substrate analog, (upper).

Table II. XPLOR Refinement and Final Model Geometry Statistics

Summary of progress of refinement. Initial fitting was done to $F_{O(complex)} - F_{O(native)}$ difference maps calculated from 15-3.0 Å using combined native phases (15-5.0 Å MIR solvent flattened phases + 5.0-2.85 Å calculated phases). Subsequent refitting was done using both this map and $2F_O - F_C$ maps with calculated phases. R-factor is defined as $(\Sigma| F_{obs} - F_{calc} |)/\Sigma F_{obs}$, where F_{obs} is the observed structure-factor amplitudes from the complex data and F_{calc} is the structure-factor amplitudes calculated from the model.

STAGE OF REFINEMENT	RESOLUTION RANGE (Å)	NUMBER OF REFLECTIONS	R-FACTOR
INITIAL MODEL: refined native human PNP model			
TCNR	8-2.9	9720	32.5
RIBAVIRIN	8-2.9	10,568	33.3
STEP I: XPLOR, simulate annealing refinement/refitting			
TCNR	8-2.9	9720	21.5
RIBIVIRAN	8-2.9	10,568	22.6
STEP II: XPLOR, conjugate gradient minimization/refitting			
TCNR	6-2.9	8807	20.8
RIBIVIRIN	6-2.9	9583	21.8
STEP III: XPLOR, conjugate gradient minimization			
TCNR	6-2.9	8807	20.8
RIBAVIRIN	6-2.9	9583	21.8

FINAL GEOMETRY	TCNR	RIBAVIRIN
RMS DEVIATION FROM IDEALITY (Å): BONDS	.014	.016
RMS DEVIATION FROM IDEALITY (°): ANGLES	1.846	1.932

Kinetic Analysis

The construction of plasmids, expression of recombinant protein, and purification of human wild-type and Asn243Asp mutant PNPs will be described elsewhere (13,18). The enzymes were purified to homogeneity and stored at -80°C. Special reagents were purchased from Sigma Chemical Co. (St. Louis, MO). Enzyme dilutions were made into a stabilizing buffer of 100 mM N-(2-hydroxyethyl)piperazine-N'-(ethanesulfonic acid), pH 7.0, 1 mM dithiothreitol, 2% polyethylene glycol 3350, and 0.02% sodium azide. Inosine phosphorolysis was monitored spectrophotometrically at 293 nm using the coupled assay (19). For inhibition studies, the 1 ml reaction volumes contained 50 mM potassium phosphate, pH 7.0, 0.07 unit xanthine oxidase (Grade III; to convert hypoxanthine to uric acid), approximately the K_m concentration of inosine, and varying concentrations of inhibitor. Reaction at 30° C was initiated by the addition of an aliquot of the enzyme solution containing 0.1 μg or 1.4 μg of wild-type or Asn243Asp protein, respectively. A linear initial reaction velocity was recorded for 2-3 min. Inhibition was assumed to be competitive as has been shown for TCNR and human lymphoblastic (7) and erythrocytic (2) PNP. The K_m value for inosine was determined with each enzyme preparation by fitting the reaction velocities at eight substrate concentrations to the Michaelis-Menten equation. Inosine concentrations ranged from 5-500 μM with wild-type PNP and from 0.06-4.8 mM with the mutant. The K_i values were obtained by fitting the percentages of inhibition caused by different inhibitor concentrations to the equation, % Inhibition = $100I/[K_i(1+S/K_m) + I]$, where I and S are the inhibitor and substrate concentrations, respectively. Inhibitors were tested at eight concentrations that ranged from 2-100 μM for TCNR and 0.5-15 mM for ribavirin. Nonlinear regression analyses of the data were carried out with the Enzfitter (Elsevier-BIOSOFT) computer program. Reaction velocities in the presence of TCNR were plotted on Dixon plots only for comparison with earlier studies (2,7).

RESULTS AND DISCUSSION

X-ray Crystallography

The refinement of both PNP complexes resulted in structures having good final geometries and R factors (Table II). In addition, the final structures produced good fit of the experimentally determined electron density for both $2F_O$-F_C maps and the original difference Fourier maps. Figure 2 shows the experimentally determined electron densities for TCNR and ribavirin bound to PNP along with final, refined models. Well-determined density for each compound is seen in the respective difference maps allowing unambiguous fitting of both nucleosides. Both compounds show a similar geometry of binding which is also similar to other PNP/nucleoside analog complexes that have been analyzed by X-ray

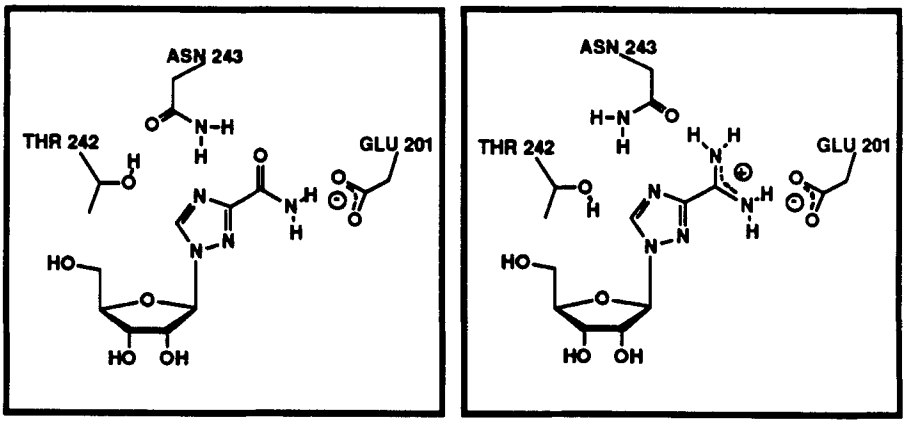

Figure 3. Proposed models of binding of ribavirin (left) and TCNR (right) by PNP. Both models hypothesize interaction between Asn 243 and the N(4) position of the triazole ring and between Glu 201 and the protonated carboxamidine of TCNR and the carboxamide of ribavirin. The protonated carboxamidine provides the potential for hydrogen bonding between the proximal nucleoside amide and the amide oxygen of Asn 243 and between the triazole N(4) and the Asn 243 amide nitrogen (the potential for the former is missing for ribavirin). Further, the protonated carboxamidine provides the potential for a strong charge-charge interaction with the Glu 201 carboxyl (also missing for ribavirin).

crystallography (4,5). Of particular interest are contacts observed in the models between Asn 243 and the triazole N(4) and between Glu 201 and the 3-carboxamide/amidine substituent. These two protein residues are believed to be particularly important for orienting the purine ring of normal substrates. In both cases described here, significant contacts are made between these residues and the nucleosides. Aside from minor differences, the electron density of both compounds is extremely similar suggesting a common binding geometry with the enzyme. In light of these observations, Figure 3 shows an interpretation of the hydrogen bonding schemes for the interactions of PNP with TCNR and ribavirin. For both TCNR and ribavirin, hydrogen bond formation is proposed between Asn 243 and N(4) of the triazole ring and between Glu 201 and the 3-carboxamide/amidine substituent of the triazole ring. In the case of the Asn 243 interaction, a 180° rotation of the Asn 243 amide between the two structures is inferred from potential hydrogen bond formation, although the two orientations cannot be experimentally differentiated. While the amide oxygen and nitrogen of Asn243 are indistinguishable at 2.9 Å resolution, the proposed models lend a biochemical basis for a stronger interaction between Asn243 and the carboxamidine of TCNR owing to better pairing of hydrogen bond donor and acceptor groups. Similarly, a stronger interaction between Glu 201 and

Table III. Kinetic Constants for Recombinant Wild-type and Asn243Asp PNP

ENZYME	NUCLEOSIDE		
	INOSINE (K_M)	TCNR (K_i)	RIBAVIRIN (K_i)
WILD-TYPE	64 μM	17.6 μM	4.9 mM
ASN243ASP	618 μM	3.8 μM	4.7 mM

the carboxamidine group of TCNR is suggested. The carboxamidine of TCNR should be protonated at physiological pH, thus presenting the potential for more favorable interaction with the negatively charged carboxyl of Glu 201, while ribavirin forms a weaker hydrogen bond with the negatively charged carboxyl of Glu 201. Biochemical evidence for such stronger binding of TCNR to PNP is also provided by the kinetic constants in Table III.

Regarding the orientation of the sugar moiety of the nucleosides, both complexes refined to a $C_{4'}$-endo conformation. In both cases, this provides a good fit to the experimentally derived electron density (Figure 2). While sugar pucker cannot be unambiguously assessed at 3.0 Å resolution, this geometry provides a better fit to the experimentally determined electron density than does the more conventional $C_{2'}$-endo-$C_{3'}$-exo conformation. Similarly, glycosidic torsion angles, χ, (defined as the angle O4'-C1'-N1-C5) were described. The final χ value for TCNR was -39° while that for ribavirin was -34°. Both are tending to the negative *syn*-clinal (-sc) region as described by Klyne and Prelog (*anti* in the Donohue and Trueblood nomenclature) which is somewhat unusual in crystallographically observed nucleic acid derivatives (20). This combination of unusual glycosidic parameters may be energetically less favorable for the C-N bond and, thus, part of the cleavage mechanism for normal substrates.

The small molecule crystal structures of ribavirin (16) and 5-amino-TCNR (6) provide conformational data for the unbound molecules, and allow a comparison of conformational features involved in substrate/analog binding to the enzyme. The observed glycosidic angles for two reported crystal forms of ribavirin were χ = 10.4° and χ = 119.0° (16). These values are within the normally observed range seen in structural studies of nucleic acid derivatives (20). Alternatively, a value of χ = -77.4° was reported for 5-amino-TCNR (6). This is an unusual conformation tending to the classical *syn* configuration which may result from the amino substitution at the 5-position. These observations suggest that PNP may selectively bind a high energy conformation of the nucleoside analog. This non-standard conformation may be stabilized by hydrogen bond interactions between the nucleoside's ribosyl O5' and His 257 and between O3' and Tyr 88 (Figure 2).

Similarly, the observed $C_{4'}$-endo sugar pucker is of "nonstandard" conformation when compared with literature values (20). For the two X-ray cystallographically determined structures of ribavirin the ribose conformations of $C_{3'}$-endo-$C_{2'}$-exo and $C_{2'}$-exo, respectively, were observed while $C_{3'}$-endo was reported for 5-aminoTCNR. Although the small molecule structures of the compounds alone may be affected by crystal packing forces, the final conformations fall in the range of normally observed values (20). Therefore the data suggest that both the nonstandard glycosidic torsion angles and nonstandard sugar pucker may be required for enzyme catalysis.

Kinetics

The inhibition constants (K_i) for TCNR and ribavirin and Michaelis constants (K_m) for inosine were determined with recombinant human wild-type PNP and the Asn243Asp mutant and are presented in Table III. The inosine analog, ribavirin, has low affinity for both enzymes whereas the adenosine analogue, TCNR, exhibits higher affinities and 4-fold tighter binding with the mutant enzyme. This contrasts with the relative substrate preferences of PNP for 6-oxo- and 6-aminopurines. The best explanation for tighter binding to PNP of TCNR relative to ribavirin comes from consideration of the interactions of the inhibitors with Glu 201. In the case of TCNR, the carboxamidine group is protonated at physiological pH and provides a salt bridge to the negatively charged Glu 201 side chain. In contrast, ribavirin forms a hydrogen bond with Glu 201 using an amino group, a relatively poor hydrogen donor. In addition, further enhancement of TCNR binding to the Asn243Asp mutant may result from the protonated carboxamidine interacting both with Glu 201 and a second negatively charged side chain provided by Asp 243. Inosine (Table III) shows 10-fold lower substrate affinity for mutant PNP relative to wild-type PNP which may result from the loss of the hydrogen bond between Asn 243 and O(6) of inosine.

The K_i values for TCNR are similar to those reported previously for human lymphocytic (5 μM (7) or 30 μM (6)) and erythrocytic (5 μM (2)) PNP. It should be noted that both those enzymes were found to exhibit cooperativity with inosine (2,6,7). The slopes of inhibition curves for TCNR were reported to be curvilinear and the K_i values were extrapolated from data obtained at low inhibitor concentrations (6,7). The recombinant human enzyme and its Asn243Asp mutant do not show cooperativity with nucleoside substrates. In the present studies and other work (13), double reciprocal plots for initial velocities over a wide range of inosine concentrations appear linear. The slopes of 1/velocity vs. inhibitor concentration plots (Dixon plots) for TCNR concentrations ranging up to 100 μM appear linear as well.

Conclusions

As truncated nucleosides, the structure of ribavirin is analogous to inosine, a natural substrates for human PNP, while the structure of TCNR is analogous to adenosine. In human PNP about 15 amino acid residues interact with and provide catalytic discrimination for nucleoside substrates. Of these, Asn 243 and Glu 201 form hydrogen bonds with the purine base, Tyr 88 and His 257 form hydrogen bonds with the ribosyl group and Ser 33, Arg 84, His 86 and Ser 220 form hydrogen bonds with the phosphate. The remaining interactions are in the form of van der Waals contacts between side chains and substrate or inhibitor. In the case of many 6-oxopurines, a conformational change occurs in residues 241-265 upon substrate or inhibitor binding. The conformational change results in a loop-helix transition for residues 257-265 which allows the active site to clasp the ligand.

X-ray crystallographic analysis shows that both TCNR and ribavirin bind to the active site of human PNP in approximately the same configuration as the corresponding nucleosides, adenosine or inosine, respectively (Figure 4). Figure 4 shows a comparison between ribavirin and 9-deazainosine, rather than inosine, because inosine is cleaved *in situ* and shows electron density only for the purine base, hypoxanthine, and not the sugar moiety (21). 9-Deazainosine was suitable for the comparison because it induces the same protein conformational changes seen with all 6-oxopurine bases and nucleosides that have been studied (21). Although small shifts are observed between the compared structures, the triazole rings occupy approximately the same position as the imidazole moieties and the ribosyl groups occupy the normal sugar binding site. However, the conformational change resulting in helix formation is not observed for either TCNR or ribavirin. Both TCNR and ribavirin appear to bind in the *syn* conformation with torsion angles of -39° and -34°, respectively. The *syn* conformation has also been observed for many other nucleoside analogs complexed with human PNP and allows the formation of hydrogen bonds between O(3') and Tyr 88 and between O(5') and His 257 and positions a nucleoside substrate for nucleophilic attack by phosphate.

Kinetics data show that TCNR (K_i = 17.6 μM) binds to human PNP with greater affinity than either inosine (K_m = 64 μM) or adenosine (K_m > 600 μM (13)). In contrast, ribavirin binds to PNP only poorly (K_i = 4.9 mM). These results can best be explained on the basis of interaction between Glu 201 and the carboxamide group of ribavirin or the carboxamidine of TCNR. In the case of ribavirin the normal N-H ··· O hydrogen bond with Glu 201 is replaced by the much weaker NH_2 ··· O hydrogen bond with the amino group of ribavirin. In the case of TCNR, the carboxamidine group, which is probably protonated at physiological pH, forms a much stronger hydrogen bond compared to substrate.

The interaction with Asn 243 occurs between the N(4) position of the triazole ring and the carboxamide of ribavirin or the carboxamidine of TCNR. For both ligands the interactions with Asn 243 are approximately the same as for the corresponding purine nucleoside. Ribavirin and TCNR were also tested as inhibitors for an Asn243Asp mutant of PNP. Mutation of Asn 243 has some effect on TCNR (K_i = 3.8 μM) since the Asp side chain can also hydrogen bond to the carboxamidine group. In the case of ribavirin the mutation has no effect on affinity, although this hydrogen bond is absent. These observations suggest that Glu 201 is primarily responsible in determining the preference of PNP for TCNR over ribavirin.

Crystallographic studies of TCNR and ribavirin complexed to human PNP provide a basis for understanding the inhibitory action of these truncated nucleoside analogs. Subsequent to the identification of TCNR as a first generation PNP inhibitor, 5-amino-TCNR (which resembles 8-aminopurines) and 5'-deoxy-TCNR were synthesized but provided no more than a three-fold improvement in affinity (6). Other families of PNP inhibitors have now been identified with K_i values in the nanomolar range. In most cases, the crystal structure of PNP provides an explanation for the activity and in some cases the structure was used to predict the binding properties of the inhibitor (5). It is hoped that the analysis presented here may lead to the development of other triazole carboxamides or carboxamidines as potent inhibitors of human PNP.

ACKNOWLEDGEMENTS

This paper is dedicated to the memory of Roland K. Robins whose laboratory first synthesized TCNR and ribavirin. This research was supported by NIH grant GM 48874, American Cancer Society grant CH-7, and Roger Williams Cancer Center CORE grant P30.CA 13943. The purification of PNP by Rose Marie Smith and the support of R.E. Parks Jr. are gratefully acknowledged.

REFERENCES

1. J C Sircar, R B Gilbertsen. *Purine Nucleoside Phosphorylase (PNP) Inhibitors: Potentially Selective Immunosuppressive Agents* in *Drugs of the Future*, 1988, **13**, 653.

2. J D Stoeckler. *Purine Nucleoside Phosphorylase: A Target for Chemotherapy* in *Developments in Cancer Chemotherapy*, R I Glazier, Ed., CRC Press, Boca Raton, FL, 1984, 33.

3. M L Markert. *Immunodeficiency Rev.*, 1991, **3**, 45.

4. S E Ealick, S A Rule, D C Carter, T J Greenhough, Y S Babu, W J Cook, J Habash, J R Helliwell, J D Stoeckler, R E Parks Jr, S-F Chen, C E Bugg. *J. Biol. Chem.*, 1990, **265**, 1812.

5. S E Ealick, Y S Babu, C E Bugg, M K Erion, W C Guida, J A Montgomery, J A Secrist III. *Proc. Natl. Acad. Sci. U.S.A.*, 1991, **88**, 11540.

6. Y S Sanghvi, N B Hanna, S E Larson, J M Fujitaki, R C Willis, R A Smith, R K Robins, G R Revankar. *J. Med. Chem.*, 1988, **31**, 330.

7. R C Willis, R K Robins, J E Seegmiller. *Mol. Pharmacol.*, 1980, **18**, 287.

8. S R Naik, J T Witkowski, R K Robins. *J. Heterocycl. Chem.*, 1974, **11**, 57.

9. R W Sidwell, J H Huffman, G P Khare, L B Allen, J T Witkowski, R K Robins. *Science.*, 1972, **177**, 705.

10. J T Witkowski, R K Robins, R W Sidwell, L N Simon. *J. Med. Chem.*, 1972, **15**, 1150.

11. R W Sidwell, R K Robins, I W Hillyard. *Pharmacol. Ther.*, 1979, **6**, 123.

12. J T Witkowski, R K Robins, G P Khare, R W Sidwell. *J. Med. Chem.*, 1973, **16**, 935.

13. J D Stoeckler, A F Poirot, R M Smith, R E Parks Jr., R L Walter, S E Ealick, S L Shames, K Takabayashi, S Wagner, M D Erion. (Unpublished results).

14. W J Cook, S E Ealick, C E Bugg, J D Stoeckler, R E Parks Jr. *J. Biol. Chem.*, 1981, **256**, 4079.

15. J Sack. *J. Mol. Graphics*, 1988, **6**, 224.

16. P Prusiner, M Sundaralingam. *Acta Cryst.*, 1976, **B32**, 419.

17. A T Brünger. *X-PLOR. Version 3.1. A System for X-ray Crystallography and NMR* , Yale University Press, New Haven, CN 1992.

18. M D Erion, W C Guida, J D Stoeckler, R L Walter, S E Ealick. (Unpublished results).

19. J D Stoeckler, R P Agarwal, K C Agarwal, R E Parks Jr. *Methods Enzymol.*, 1978, **51**, 530.

20. M Sundaralingam. *Biopolymers*, 1969, **7**, 821.

21. S E Ealick, J S Symersky, R L Walter. (Unpublished results).

Received 8/18/93
Accepted 11/3/93